Inferring generation-interval distributions from contact-tracing data

Sang Woo Park[1,*] David Champredon[2,3] Jonathan Dushoff[2,4]

1 Department of Mathematics & Statistics, McMaster University, Hamilton, Ontario, Canada
2 Department of Biology, McMaster University, Hamilton, Ontario, Canada
3 Agent-Based Modelling Laboratory, York University, Toronto, Ontario, Canada
4 Michael G. DeGroote Institute for Infectious Disease Research, McMaster University, Hamilton, Ontario, Canada

*parksw3@mcmaster.ca

Abstract

Generation intervals, defined as the time between when an individual is infected and when that individual infects another person, link two key quantities that describe an epidemic: the reproductive number, $\mathcal{R}$, and the rate of exponential growth, r. Generation intervals are often measured through contact tracing by identifying who infected whom. We study how observed intervals differ from "intrinsic" intervals that could be estimated by tracing individual-level infectiousness, and identify both spatial and temporal effects, including censoring (due to observation time), and the effects of susceptible depletion at various spatial scales. Early in an epidemic, we expect the variation in the observed generation intervals to be mainly driven by the censoring and the population structure near the source of disease spread; therefore, we predict that correcting observed intervals for the effect of temporal censoring but *not* for spatial effects will provide a spatially informed "effective" generation-interval distribution, which will correctly link r and $\mathcal{R}$. We develop and test statistical methods for temporal corrections of generation intervals, and confirm our prediction using individual-based simulations on an empirical network.

Keywords

Infectious disease modeling, generation interval, basic reproduction number, population structure, contact tracing

1 Introduction

An epidemic can be characterized by the exponential growth rate, r, and the reproductive number, $\mathcal{R}$. The reproductive number, defined as the average number of secondary cases arising from a primary case, is of particular interest as it provides information about the final size of an epidemic (Anderson and May, 1991; Diekmann et al., 1990). However, estimating the reproductive number directly from disease natural history requires detailed knowledge which is not often available, particularly early in an outbreak (Dietz, 1993). Instead, the reproductive number can be *indirectly* estimated from the exponential growth rate, which can be estimated from incidence data (Chowell et al., 2003; Mills et al., 2004; Nishiura et al., 2009, 2010; Ma et al., 2014). These two quantities are linked by generation-interval distributions (Wearing et al., 2005; Svensson, 2007; Roberts and Heesterbeek, 2007; Wallinga and Lipsitch, 2007; Park et al., 2019).

A generation interval is defined as the time between when a person becomes infected and when that person infects another person (Svensson, 2007). Due to individual variation in infection time, the observed generation-interval distribution can change depending on when and how it is measured (Svensson, 2007; Kenah et al., 2008; Nishiura, 2010; Champredon and Dushoff, 2015). There are important distinctions to be made when estimating generation intervals: *intrinsic* generation intervals measure the infectiousness of an infected individual, while *observed* generation intervals refer to the time between actual infection events. Observed generation intervals in turn can be measured either *forward* in time by looking at a cohort of individuals infected at the same time and asking when they infected others or *backward* in time by looking at a cohort and asking when their infectors were infected (Champredon and Dushoff, 2015).

While the intrinsic generation-interval distribution is often assumed to be fixed, the shape of the observed generation-interval distribution depends on when and how intervals are measured (Kenah et al., 2008; Nishiura, 2010; Scalia Tomba et al., 2010; Champredon and Dushoff, 2015; Britton and Scalia Tomba, 2019). Here, we briefly describe how backward generation-interval distributions change over time because backward measurements better reflect real outbreak scenarios where contact tracing is performed by identifying infectors of infected individuals. (see Kenah et al. (2008); Nishiura (2010); Scalia Tomba et al. (2010); Champredon and Dushoff (2015) for discussions on forward generation intervals). When an epidemic is growing exponentially, as often occurs near the beginning of an outbreak, the number of newly infected individuals will be large relative to the number infected earlier on. A susceptible individual is thus relatively more likely to be infected by a newly infected individual, and the distribution of backward generation intervals will be shorter than the intrinsic distribution (Nishiura, 2010; Champredon and Dushoff, 2015; Britton and Scalia Tomba, 2019). When an epidemic is subsiding, most infections are caused by the remaining infectors, rather than new infectors, and backward generation intervals will be longer than the intrinsic one (Nishiura, 2010; Scalia Tomba et al., 2010; Champredon and Dushoff, 2015).

In practice, generation intervals are often measured by aggregating available information from contact tracing. While an epidemic is ongoing, these measurements are "censored":

we don't know what happens after the observation time. Thus, there is a bias towards observing shorter intervals, which are more likely to have concluded by the observation time. In fact, censored observations can be thought of as an average of backward generation-interval distributions, over the cohorts which have been infected before the observation time (and weighted by cohort size).

Realized generation intervals are also affected by spatial structure. In a structured population (that is, any population that does not mix homogeneously), susceptibility will tend to decrease more quickly in the neighbourhood of infected individuals than in the general population even in the early phase of an epidemic. This means that contacts made late in an individual's infection are more likely to be ineffective due to contacts that were made earlier (because the contactee may have been infected already) As a result, realized generation intervals will have shorter mean than the intrinsic generation-interval distribution. This perspective allows us to reinterpret the finding of Trapman et al. (2016) that, given an intrinsic generation interval and an observed growth rate, the reproductive number on various network structures is always smaller on a network than would be predicted from homogeneous mixing. These observations allow us to make the following prediction: removing the time-censoring bias from observed generation intervals will give us a corrected distribution that contains information about the population structure; using this corrected distribution should allow us to correctly infer the reproductive number from the exponential growth rate. In other words, Trapman *et al.*'s finding can be explained by the gap between the intrinsic generation interval and an "effective" (spatially corrected) generation interval.

In this study, we explore spatiotemporal variation in generation intervals measured through contact tracing. We extend previous frameworks to study how the censored generation-interval distributions change over time and compare this distribution with the backward generation-interval distribution. We classify sources of spatial variation in generation intervals into three levels (egocentric, local, and global) and discuss how they affect observed generation-interval distributions. Finally, we compare two methods for accounting for temporal bias and test our prediction using simulations.

2 Intrinsic generation-interval distributions

Generation-interval distributions are often considered as population averages, but we can distinguish population-level distributions from individual-level distributions (Svensson, 2007, 2015); making this distinction clear will be particularly useful when we discuss spatial components (see Fig. 1). An individual-level intrinsic infection kernel $k(\tau; a)$ describes the rate at which an infected individual with "aspect" a makes "effective contacts" (contacts which will cause infection if the contactee is susceptible). Individual aspects may represent variation in the course of infection (e.g., duration of latent and infectious periods) and the level of infectiousness, which can depend both on biological infectiousness as well as contact patterns.

Assuming that the individual properties are independent of risk of infection, the population-

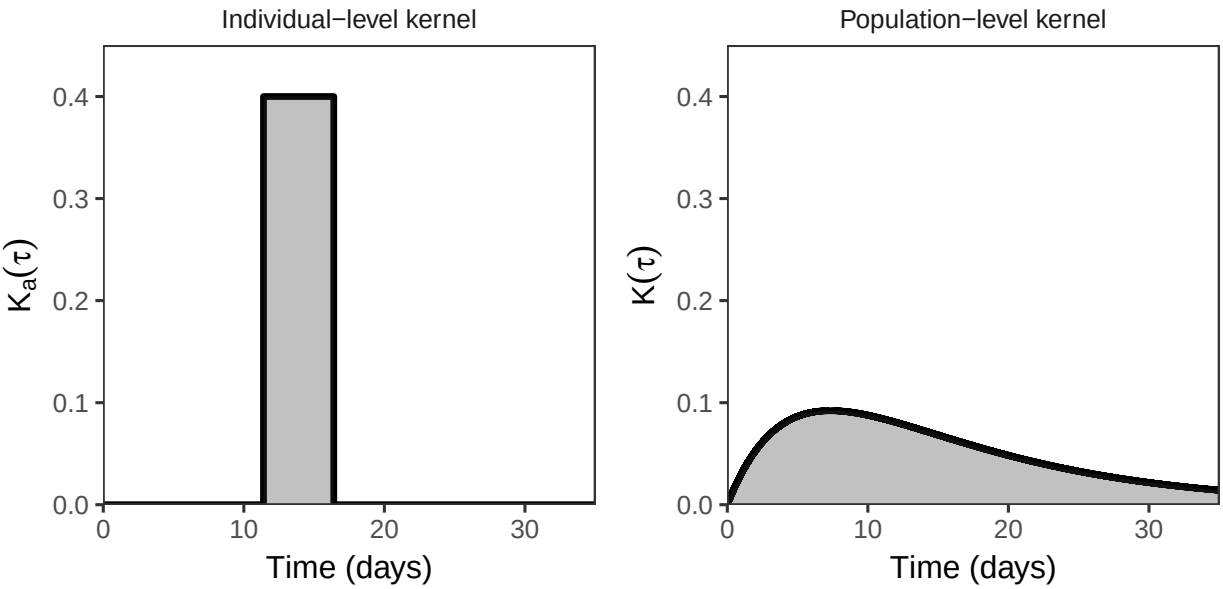

Figure 1: **Comparison of individual- and population-level kernels.** (Left) an individual-level kernel of an infected individual with latent period of 11.4 days followed by infectious period of 5 days. (Right) a population-level kernel of infected individuals with latent and infectious periods exponentially distributed with means of 11.4 and 5 days, respectively. Shaded areas under the curves are equal to individual- and population-level reproductive numbers, both of which are set to 2 in this example. Parameters are chosen to reflect the West African Ebola outbreak (WHO Ebola Response Team, 2014).

level kernel is given by integrating over these individual variations:

$$K(\tau) = \int k(\tau; a) f(a) da, \tag{1}$$

The population-level kernel describes the rate at which secondary infections are expected to be caused by an an infected individual, on *average*. where $f(a)$ represents a probability density over a (possibly multi-dimensional) aspect space.

Assuming that a population mixes homogeneously, we can write:

$$K(\tau) = \mathcal{R}_0 g(\tau), \tag{2}$$

where $\mathcal{R}_0 = \int K(\tau) d\tau$ is the basic reproductive number (the expected number of secondary cases caused by a randomly chosen infectious individual in a fully susceptible population), and $g(\tau)$ is the expected time distribution of those cases (the intrinsic generation-interval distribution).

In a homogeneously mixing population, current disease incidence at time t, $i(t)$, is the product of the current infectiousness of individuals infected in the past and the current proportion of the population susceptible, $S(t)$.

$$i(t) = S(t) \int K(s) i(t-s) ds = \mathcal{R} \int g(s) i(t-s) ds, \tag{3}$$

where $\mathcal{R} = S(t)\mathcal{R}_0$ is the effective reproductive number. This model, also referred to as the renewal equation, can describe a wide range of epidemic models (Heesterbeek and Dietz, 1996; Diekmann and Heesterbeek, 2000; Roberts, 2004; Aldis and Roberts, 2005; Wallinga and Lipsitch, 2007; Roberts and Heesterbeek, 2007). Over a period of time where the proportion of susceptible S remains roughly constant, we would expect approximately exponential growth in incidence $i(t)$; assuming $i(t) = i(0)\exp(rt)$ yields the Euler-Lotka equation (Lotka, 1907), which provides a direct link between speed and strength of an epidemic:

$$\frac{1}{\mathcal{R}} = \int g(s) \exp(-rs) ds. \tag{4}$$

3 Generation-interval distributions across time

When generation intervals are estimated through contact tracing during an outbreak, infection events that have not happened yet are not observed. This effect is called "right-censoring". We can understand the effect of right-censoring using backward generation-interval distributions (Scalia Tomba et al., 2010; Nishiura, 2010; Champredon and Dushoff, 2015; Britton and Scalia Tomba, 2019): the observed (censored) generation-interval distribution is a weighted average of backward generation-interval distributions (weighted by incidence) up until the observation time.

The density of new infections occurring at time t caused by infectors who were infected at time $t - \tau$ is given by

$$i_{t-\tau}(t) = \mathcal{R}\, i(t-\tau) g(\tau) S(t) \tag{5}$$

As shown in Champredon and Dushoff (2015), the backward generation-interval distribution, $b_t(\tau)$, describes a distribution of infection that occurred τ time units before the reference time t and is proportional to $i(t-\tau)g(\tau)$:

$$b_t(\tau) = \frac{i(t-\tau)g(\tau)}{\int_0^t i(t-\sigma)g(\sigma)d\sigma} \tag{6}$$

On the other hand, the censored generation-interval distribution, $c_t(\tau)$, describes a distribution of *all* infections that are τ time units apart from any cohort infected at time s before t: $\int_0^t i_{s-\tau}(s)ds$. Then, the censored generation-interval distribution is given by normalizing

$$c_t(\tau) = \frac{\int_0^t i_{s-\tau}(s)ds}{\int_0^t \int_0^t i_{s-\sigma}(s)dsd\sigma} = \frac{\int_0^t i(s-\tau)g(\tau)S(s)ds}{\int_0^t \int_0^t i(s-\sigma)g(x)S(s)dsd\sigma} \tag{7}$$

Substituting (6) allows us to rewrite the censored generation-interval distribution as a weighted distribution of the backward generation intervals:

$$c_t(\tau) \propto \int_0^t b_s(\tau)i(s)ds. \tag{8}$$

For a single outbreak, the observed mean generation interval through contact tracing will always be shorter than the mean intrinsic generation interval (Figure 2). There are two reasons for this phenomenon. First, longer generation intervals are more likely to be missed due to right censoring (and short generation intervals are more likely to be observed). In particular, when an epidemic is growing exponentially ($i(t) = i(0)\exp(rt)$), the censored generation-interval distribution (as well as the backward generation-interval distribution) can be written as the intrinsic generation-interval distribution discounted by the rate of exponential growth (Britton and Scalia Tomba, 2019):

$$c_0(\tau) = b_0(\tau) \propto g(\tau)\exp(-r\tau), \tag{9}$$

where c_0 and b_0 represent the "initial" censored and backward generation-interval distributions (during the exponential growth phase), respectively. A deterministic simulation confirms that the censored generation-interval distribution has the same mean as the backward generation-interval distribution during this period (Figure 2). Second, the decreasing number of susceptibles over the course of an epidemic makes long infections less likely to occur (Champredon and Dushoff, 2015). As a result, even if contact tracing is performed through an entire epidemic, the mean intrinsic generation interval will be underestimated. Long backward generation intervals near the end of an epidemic have little effect on the censored generation-interval distributions because they represent only a small portion of an outbreak. Overall, we expect, naively using the observed generation-interval distribution, to underestimate the reproductive number.

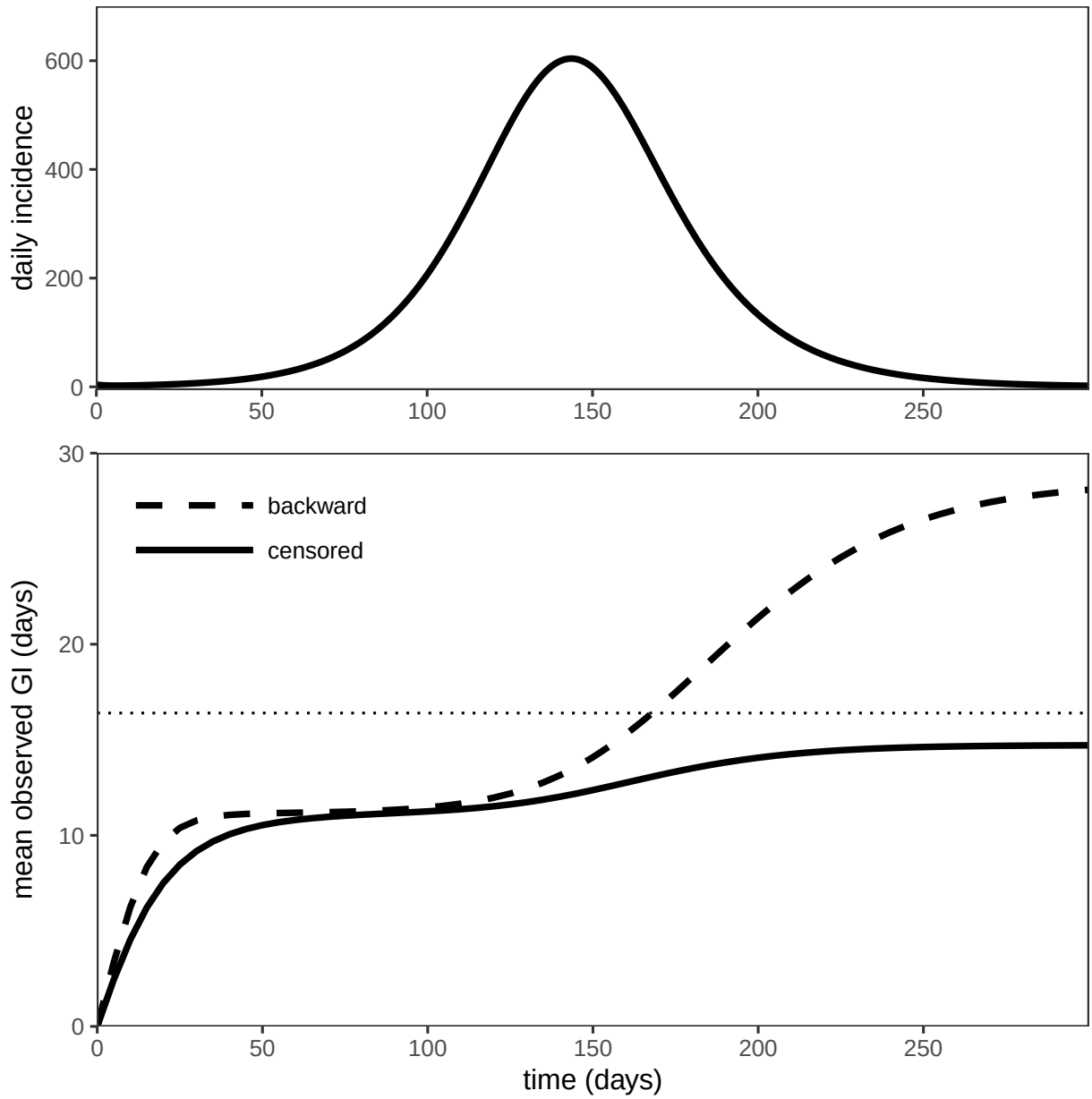

Figure 2: **Temporal variation in the mean observed generation interval.** A deterministic Susceptible-Exposed-Infectious-Recovered (SEIR) model was simulated using Ebola-like parameters (WHO Ebola Response Team, 2014): mean latent period $1/\sigma = 5$ days, mean infectious period $1/\gamma = 11.4$ days, and the basic reproductive number $\mathcal{R}_0 = 2$. The backward and the censored mean generation interval were calculated over the course of an epidemic. The dotted horizontal line represents the mean intrinsic generation interval.

4 Generation-interval distributions across space

Infected individuals may contact the same susceptible individual multiple times, but only the first effective contact gives rise to infection in a given individual (after this, they are no longer susceptible). Therefore, we expect realized generation intervals to be shorter than intrinsic generation intervals, on average, in a limited contact network.

To explore the effect of multiple contacts on realized generation intervals, we first consider the infection process from an "egocentric" point of view, taking into account infectious contacts made by a single infector. We define the egocentric kernel as the rate at which secondary infections are realized by a single primary case with aspect a in the absence of other infectors:

$$\hat{k}(\tau; a) = k(\tau; a) \exp\left(-\delta(a) \int_0^\tau k(s; a) ds\right), \tag{10}$$

where $k(\tau; a)$ is the individual-level intrinsic kernel and $e^{-\delta(a)\int_0^\tau k(s;a)ds}$ is the probability that a susceptible acquaintance has not yet been contacted by a particular infected individual. The dilution term, $\delta(a)$, models how contacts are distributed among susceptible acquaintances.

Throughout this paper, we assume that there is a constant per-pair contact rate λ. In this case, the infectiousness of an individual $\mathcal{R}(a) = \int k(s; a) ds$ is the product of the number of acquaintances $N(a)$ and the contact rate λ; the dilution term is equal to the reciprocal of the number of acquaintances: $\delta(a) = 1/N(a)$. This assumption can be relaxed by allowing for asymmetry (Trapman et al., 2016) or heterogeneity (Ball et al., 1997; Ball and Neal, 2002) in contact rates; for brevity, we do not pursue these directions here.

The population-level egocentric kernel is found by integrating over individual variations:

$$\hat{K}(\tau) = \int \hat{k}(\tau; a) f(a) da. \tag{11}$$

Trapman et al. (2016) used this same kernel (also assuming a constant per-pair contact rate) to study the effect of network structure on the estimate of reproductive number. The population-level egocentric generation-interval distribution is:

$$\hat{g}(\tau) = \frac{\hat{K}(\tau)}{\int \hat{K}(s) ds}. \tag{12}$$

The population-level egocentric generation-interval distribution describes the distribution of times at which secondary infections are realized by an *average* primary case; for convenience, we will often omit "population-level". Finally, the link between the growth rate and the egocentric reproductive number are linked by the egocentric generation-interval distribution (and the Euler-Lotka equation) (Trapman et al., 2016):

$$\frac{1}{\hat{\mathcal{R}}} = \int \hat{g}(\tau) \exp(-r\tau) d\tau. \tag{13}$$

As the egocentric distribution always has a shorter mean than the intrinsic distribution, $\hat{\mathcal{R}}$ will always be smaller than $\mathcal{R}$ estimated from the intrinsic distribution; this generation-interval-based argument provides a clear biological interpretation for the result presented by Trapman et al. (2016).

For example, consider a susceptible-exposed-infected-recovered (SEIR) model, which assumes that latent and infectious periods are exponentially distributed. The intrinsic generation-interval distribution that corresponds to this model can be written as (Champredon et al., 2018):

$$g(\tau) = \frac{\sigma\gamma}{\sigma - \gamma}\left(e^{-\gamma t} - e^{-\sigma t}\right), \tag{14}$$

where $1/\sigma$ and $1/\gamma$ are mean latent and infectious periods, respectively. Assuming a constant per-pair contact rate of λ for any pair, we obtain the following egocentric generation-interval distribution:

$$\hat{g}(\tau) = \frac{\sigma(\gamma + \lambda)}{\sigma - (\gamma + \lambda)}\left(e^{-(\gamma+\lambda)\tau} - e^{-\sigma\tau}\right) \tag{15}$$

In this case, with fixed infectiousness during the infection period, the effect of accounting for pairwise contacts is the same as an increase in the recovery rate (by the amount of the per-pair contact rate): infecting a susceptible contact is analogous to no longer being infectious (since the contact cannot be infected again); therefore, the resulting egocentric generation-interval distribution is equivalent to the intrinsic generation-interval distribution with mean latent period of $1/\sigma$ and mean infectious period of $1/(\gamma+\lambda)$. In practice, directly using this distribution to link r and $\mathcal{R}$ using the Euler-Lotka equation is unrealistic because it requires that we know the per-pair contact rate. Instead, the per-pair contact rate can be inferred from the growth rate r, assuming that mean and variance of the degree distribution of a network is known (see Trapman et al. (2016) supplementary material section 1.4.2); we briefly describe this relationship in Section 7.3.

This calculation can be validated by simulating stochastic infection processes on a "star" network (i.e, a single infected individual at the center connected to multiple susceptible individuals who are not connected with each other). Simulations (Fig. 3) confirm that in this case the distribution of *contact* times matches the intrinsic generation-interval distribution (left panel), while the distribution of realized generation times (i.e., *infection* times) matches the egocentric generation-interval distribution (middle panel).

The egocentric generation interval (12) only explains some of the reduction in generation times that occurs on most networks, however. Generation intervals are also shortened by indirect connections: a susceptible individual can be infected through another route before the focal individual makes infectious contacts. Simulations on a small homogeneous network confirm this additional effect (Fig. 3, right panel).

In general, spatial reduction in the mean generation interval can be viewed as an effect of susceptible depletion and can be further classified into three levels: egocentric, local, and global. Egocentric depletion, as discussed previously, is caused by an infected individual making multiple contacts to the same individual. Local depletion refers to a depletion of susceptible individuals in a household or neighborhood; we can think of these structures as small homogeneous networks embedded in a larger population structure (and therefore we

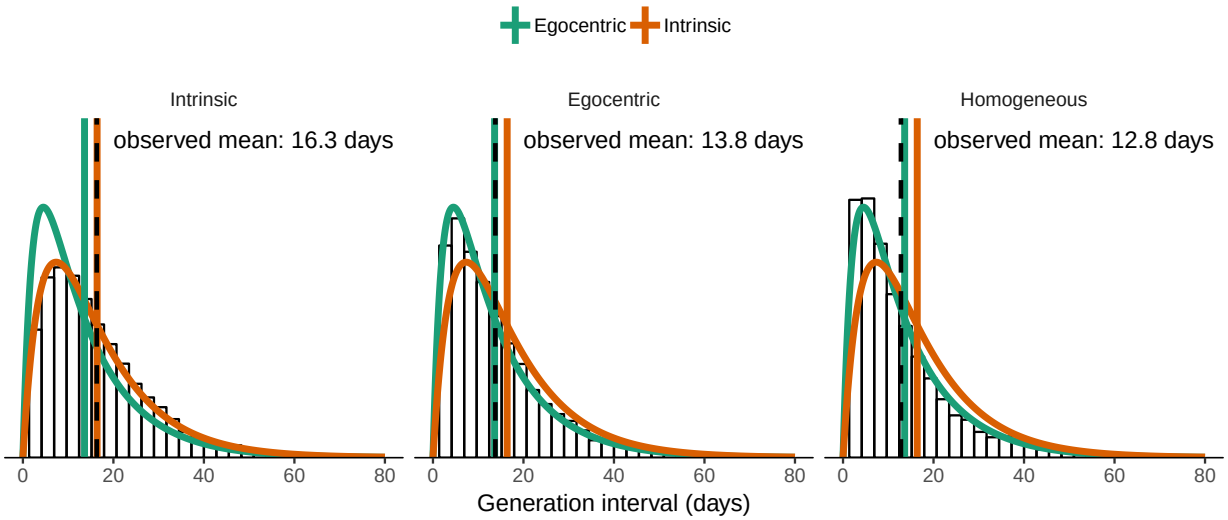

Figure 3: **Spatial effects on realized generation intervals.** Theoretical distributions and means are shown in color (and are the same in each panel, for reference). Simulated distributions and means are shown in black. (Left) the intrinsic generation-interval distribution corresponds to all contacts by a focal individual, regardless of whether the individual contacted is susceptible (simulated on a star network). (Middle) the egocentric generation-interval distribution corresponds to the distribution of all infectious contacts by the focal individual with susceptible individuals, in the case where the focal individual is the only possible infector (simulated on a star network). (Right) realized generation-interval distributions are shorter than egocentric distributions in general, because contacts can be wasted when susceptibles become infected through other routes (simulated on a homogeneous network). All figures were generated using 5000 stochastic simulations on a network with 5 nodes (1 infector and 4 susceptibles) with Ebola-like parameters (WHO Ebola Response Team, 2014): mean latent period $1/\sigma = 5$ days and mean infectious period $1/\gamma = 11.4$ days. Per-pair contact rate $\lambda = 0.25$ days^{-1} is chosen to be sufficiently high so that the differences between generation-interval distributions are clear. Each simulation is run until all individuals are either susceptible or has recovered.

can expect similar effects as we see in Fig. 3, right panel). Both the egocentric and local depletion effects can be observed early in an epidemic, especially in a highly structured population, even if most of the population remains susceptible. Finally, global depletion refers to overall depeletion of susceptibility at the population level, and explains the reduction in realized compared to intrinsic generation intervals that occurs even in a well-mixed population (Fig. 2).

5 Inferring generation-interval distributions from contact-tracing data

When generation intervals are sampled through contact tracing, there will be four effects present in the sample: (1) right-censoring effect, (2) egocentric depletion effect, (3) local depletion effect and (4) global depletion effect. We can correct explicitly for the egocentric effect and, in the case of exponential growth, the right-censoring effect. While the other two effects are difficult to measure, we can make qualitative predictions about their effects on the realized generation intervals and reproductive numbers: both local and global depletion effects reduce number of infections that occur and shorten generation intervals.

Since the right-censoring effect is a sampling bias, we typically want to correct for it. In contrast, spatial effects have the same effect on how the epidemic spreads as they do on observed generation intervals. We therefore expect that starting from observed generation intervals and correcting for the right-censoring effect, will allow us to estimate an "effective" generation interval that accurately reflects dynamics of spread. When temporal correction is performed early in an outbreak, during the exponential growth phase, the effective distribution should incorporate egocentric and local spatial effects but not the global effects; we expect this distribution to correctly link r and $\mathcal{R}$. We will call the temporally corrected effective generation-interval distribution $g_{\text{eff}}(\tau)$. In a large homogeneously mixing population, the effective distribution is expected to be equivalent to the intrinsic distribution (since the egocentric and local depletion are negligible in the absence of network structure, and global depletion is negligible early in the epidemic).

Here, we investigate two methods for correcting for temporal bias in contact-tracing data (see Methods for details). We refer to the first method (Section 7.4) as the population-level method as it relies on the observed distribution aggregated across the entire population. When an epidemic is growing exponentially, right-censoring causes the observed generation interval to be discounted by the exponential growth rate (9); hence, we can "undo" the censoring by exponentially weighting the observed generation-interval distribution (Scalia Tomba et al., 2010; Nishiura, 2010; Britton and Scalia Tomba, 2019):

$$g_{\text{eff}}(\tau) \propto c_t(\tau) \exp(r\tau), \tag{16}$$

where r is the exponential growth rate.

We refer to the second method (Section 7.5) as the individual-level method because it relies on individual contact information. We model each infection as a non-homogeneous

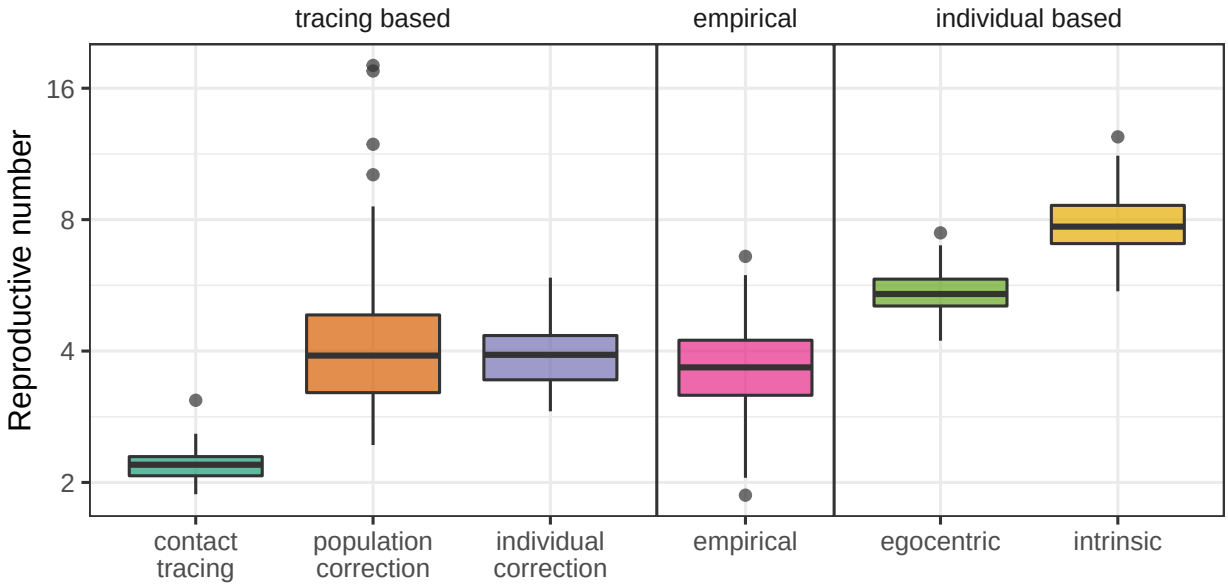

Figure 4: **Comparison of estimates of reproductive number based on various methods.** Using the observed generation-interval distributions (based on the first 1000 generation intervals) without correcting for right-censoring severely underestimates the reproductive number. Similarly, using the intrinsic generation-interval distribution overestimates the reproductive number because it fails to account for local spatial effects; the egocentric distribution corrects for this only partially. Both population-level and individual-level methods provide estimates of reproductive number that are consistent with the empirical estimates, which we define as the average number of secondary cases generated by the first 100 infected individuals, but the individual-level method is more precise. Boxplots are generated using 100 stochastic simulations of the SEIR model on an empirical network using Ebola-like parameters (WHO Ebola Response Team, 2014): mean latent period $1/\sigma = 5$ days and mean infectious period $1/\gamma = 11.4$ days. Per-pair contact rate $\lambda = 0.08$ days^{-1} is chosen to be sufficiently high such that differences are clear.

Poisson process arising from the infector (25); incorporating information about time of infection of an infector, time of infection of an infectee, and time since the beginning of an epidemic allows us to explicitly model the censoring process in the observed generation intervals. For both methods, mean and coefficient of variation (CV) of generation-interval distributions are estimated by maximum likelihood; the inferred generation-interval distribution is then used to estimate the reproductive number $\mathcal{R}$ from the observed growth rate r using the Euler-Lotka equation.

To test these methods, we simulate 100 epidemics with Ebola-like parameters on an empirical network (Leskovec and Krevl, 2014) and compare the estimates of reproductive number with empirical reproductive numbers, which we define as the average number of secondary cases generated by the first 100 infected individuals (Fig. 4). As expected, calculating reproductive number based on the intrinsic generation-interval distribution overestimates the empirical reproductive number; estimates based on the egocentric generation-interval distribution (12) address this problem only partially, as they do not account for indirect (local) spatial effects. Direct estimates based on the observed generation intervals from contact tracing severely underestimate the empirical estimates. While both population- and individual-level corrections provide similar estimates to the empirical reproductive number on average, population-level estimates are more variable as they are more sensitive to outliers in generation intervals and our estimate of the growth rate. For smaller values of $\mathcal{R}$, we expect the differences to become smaller. In Appendix, we present the same figure using smaller $\mathcal{R}$ (Appendix A.1) and using Erlang-distributed latent periods (Appendix A.2), which better corresponds to Ebola. Overall, our qualitative conclusions do not change.

6 Discussion

The intrinsic generation-interval distribution, which describes the expected time distribution of secondary cases, provides a direct link between speed (exponential growth rate, r) and strength (reproductive number, $\mathcal{R}$) of an epidemic (Wallinga and Lipsitch, 2007; Svensson, 2007, 2015; Park et al., 2019). However, observed generation-interval distributions can vary depending on how and when they are measured (Nishiura, 2010; Scalia Tomba et al., 2010; Champredon and Dushoff, 2015; Britton and Scalia Tomba, 2019); determining which distribution correctly links r and $\mathcal{R}$ can be challenging. Here, we analyze how observed generation intervals, measured through contact tracing, differ from intrinsic generation intervals. Changes due to temporal censoring reflect observation bias, whereas changes due to spatial or network structure reflect the dynamics of the outbreak. Thus, correcting the observed distribution for temporal, but not spatial, effects provides the correct link between r and $\mathcal{R}$.

Observed generation intervals are subject to right-censoring – it is not possible to trace individuals that have not been infected yet. These right-censored distributions can be thought of as averages of "backward" generation intervals (measured by tracing the infectors of a cohort of infected individuals) (Kenah et al., 2008; Nishiura, 2010; Scalia Tomba et al., 2010; Champredon and Dushoff, 2015; Britton and Scalia Tomba, 2019). During an ongoing out-

break, the observed generation-interval distribution will always have a shorter mean than the intrinsic-interval distribution due to right-censoring. Early in the outbreak, censored intervals are expected to match the early-outbreak backward intervals. Near the end of an outbreak, the effect of right-censoring becomes negligible but the observed generation intervals are still shorter on average than intrinsic generation intervals, because of depletion of the susceptible population.

We think of susceptible depletion as operating on three levels: egocentric, local, and global. Egocentric susceptible depletion refers to the effect of an infected individual making multiple contacts to the same susceptible individual. Accounting for the egocentric effect allowed us to link the results by Trapman et al. (2016) to established results based on generation intervals. Local susceptible depletion refers to the effect of other closely related infected individuals (e.g., in a household or neighborhood) making multiple contacts to the same susceptible individual. Global susceptible depletion refers to the overall decrease in the susceptible pool in the population.

Susceptible depletion happening at all three levels shortens realized generation intervals but acts on different time scales. Egocentric and local depletion effects are present from the beginning of an epidemic, even when depletion in the global susceptible population is negligible, and can strongly affect the initial spread of an epidemic. Therefore, we predicted the observed generation intervals during an exponential growth phase to contain information about the contact structure, allowing us to estimate the *effective* generation-interval distribution by simply accounting for the right-censoring. Simulation studies confirmed our prediction: using the effective generation-interval distribution provides the correct link between r and $\mathcal{R}$.

We compare two methods for estimating the effective generation-interval distribution and assume that the effective generation-interval distribution follows a gamma distribution. The gamma approximation of the generation interval distribution has been widely used due to its simplicity (McBryde et al., 2009; Nishiura et al., 2009; Roberts and Nishiura, 2011; Trichereau et al., 2012; Nishiura and Chowell, 2015); we previously thought that summarizing the entire distribution with two moments (mean and variance) is sufficient to understand the role of generation-interval distributions in linking r and $\mathcal{R}$ (Park et al., 2019). However, further investigation of our methods suggests that making a wrong distributional assumption can lead to biased estimates of the mean and CV of a generation-interval distribution (Appendix A.3), even though the gamma distribution "looks" indistinguishable from the shape of the intrinsic generation-interval distribution (derived from the SEIR model). These results are particularly alarming because it is impossible to know the true shape of the generation-interval distribution for real diseases. Nonetheless, biases in the parameter estimates of a generation-interval distribution may cancel out and give unbiased estimate of the reproductive number (Appendix A.3).

Generation-interval-based approaches to estimating the reproductive number often assume that an epidemic grows exponentially (Wearing et al., 2005; Wallinga and Lipsitch, 2007; Roberts and Heesterbeek, 2007; Park et al., 2019). In practice, heterogeneity in population structure can lead to subexponential growth (Szendroi and Csányi, 2004; Chowell et al., 2015; Chowell and Viboud, 2016; Chowell et al., 2016; Kiskowski and Chowell, 2016;

Viboud et al., 2016); we therefore expect our simulations on an empirical network to be better characterized by subexponential growth models (Viboud et al., 2016). However, our simulations suggest that the initial exponential growth assumption still provides a viable approach for estimating the reproductive number.

Contact tracing provides an effective way of collecting epidemiological data and controlling an outbreak (Clarke, 1998; Eames and Keeling, 2003; Donnelly et al., 2003). In particular, using tracing information allows us to infer real-time estimates of the time-varying reproductive number (Cauchemez et al., 2006; Hens et al., 2012; Jewell and Roberts, 2012; Soetens et al., 2018); generation-interval distributions, which can be either assumed or estimated, often play a central role in analyzing tracing data. Our study illustrates that generation intervals measured through contact-tracing data contain information about the underlying contact structure, which can be implicitly reflected in the estimates of the reproductive number; this perspective can be particularly useful for characterizing an epidemic because detailed information about the contact structure is often unavailable.

The generation-interval distribution is a key, and often under-appreciated, component of disease modeling and forecasting. Different definitions, and different measurement approaches, produce different estimates of these distributions. We have shown that estimates based on observed generation intervals (e.g., through contact tracing) differ in predictable ways from estimates based on underlying measures of infectiousness (e.g., from shedding studies). These predictable differences can arise from temporal effects, egocentric spatial effects, local spatial (or network) effects and population-level effects. We have shown that correcting observed intervals for temporal effects allows us to estimate a spatially informed "effective" distribution, which accurately describes how disease spreads in a population. Future studies should carefully consider how measurement influences estimated generation-interval distributions, and how these distributions influence the spread of disease.

7 Methods

7.1 Deterministic SEIR model

To study the effects on right-censoring on the observed generation intervals, we use the deterministic Susceptible-Exposed-Infectious-Recovered (SEIR) model. The SEIR model describes how disease spreads in a homogeneously mixing population; it assumes that infeceted individuals become infectious after a latent period. We use a $\mathrm{SE}^m\mathrm{I}^n\mathrm{R}$ model, which extends the SEIR model to have multiple equivalent stages in the latent and infectious periods. This gives latent and infectious periods with Erlang distributions (gamma distributions with integer shape parameters), which are often more realistic than the exponentially distributed

periods in the standard SEIR model (Anderson and Watson, 1980; Bailey, 1964):

$$
\begin{aligned}
\frac{dS}{dt} &= -\beta S \frac{\sum_{k=1}^{n_I} I_k}{N} \\
\frac{dE_1}{dt} &= \beta S \frac{\sum_{k=1}^{n_I} I_k}{N} - n_E \sigma E_1 \\
\frac{dE_m}{dt} &= n_E \sigma (E_{m-1} - E_m) \qquad \text{for } m = 2, 3, \ldots, n_E \\
\frac{dI_1}{dt} &= n_E \sigma E_m - n_I \gamma I_1 \\
\frac{dI_n}{dt} &= n_I \gamma (I_{n-1} I_n) \qquad \text{for } n = 2, 3, \ldots, n_I
\end{aligned}
\tag{17}
$$

where S is the number of susceptible individuals, E_m is the number of exposed individuals in the m-th compartment, I_n is the number of infectious individuals in the n-th compartment, and R is the number of recovered individuals. Parameters of the model are specified as follows: N is the total population size, β is the transmission rate, $1/\sigma$ is the mean latent period, n_E is the number of latent compartments, $1/\gamma$ is the mean infectious period, and n_I is the number of infectious compartments. While we use the SEIR model for simulations in our main text, we show results based on more realistic distributions in Appendix.

7.2 Stochastic SEIR model

We develop an algorithm to simulate an individual-based SEIR model on a network to keep track of generation intervals. Our algorithm is based on the Gillespie algorithm (Gillespie, 1977). We model individuals with nodes on a network and their acquaintanceships with edges; infected individuals can only contact their acquaintances.

First, we begin by randomly selecting initially infected individuals; these individuals are assumed to be infected at $t = 0$. For each infected individual i, we randomly draw the latent period E_i from an Erlang distribution with mean $1/\sigma$ and shape n_E. We then construct the random infectious period and infectious contact times simultaneously as follows. For each of the n_I stages of the infectious period, we draw the number of effective contacts (before transitioning to the next compartment) from a geometric distribution with probability $n_I\gamma/(S_i\lambda + n_I\gamma)$, where S_i is the number of susceptible acquaintances and λ is the per-pair contact rate. We then choose the time between consecutive events (the chosen number of contacts, followed by exit from the given stage of infection) from an exponential distribution with rate $S_i\lambda + n_I\gamma$. For each contact, a contactee is uniformly sampled from the set of susceptible acquaintances of the individual i. The infectious period I_i is the sum of all of these waiting times.

After repeating the contact process for all initially infected individuals, all contacts are put into a sorted queue. The first person in the queue becomes infected, and the current time is updated to infection time of this individual. Any subsequent contacts made to this individual are removed from the queue because they will no longer be effective. We repeat the contact process for this newly infected individual. Then, new contacts are added to

the sorted queue. The simulation continues until there are no more contacts are left in the queue.

7.3 Egocentric relationship between r and $\mathcal{R}$ (SEIR model)

Here, we show that the egocentric relationship between r and $\mathcal{R}$ derived by Trapman Trapman et al. (2016) (see the original source for detailed derivations) can be derived simply by applying the Euler-Lotka equation and using the effective (rather than the intrinsic) generation-interval distribution. Assume that latent and infectious periods are exponentially distributed with mean $1/\sigma$ and $1/\gamma$, respectively. Assuming a constant per-pair contact rate of λ for any pair, the egocentric generation-interval distribution can be written:

$$\hat{g}(\tau) = \frac{\sigma(\gamma+\lambda)}{\sigma-(\gamma+\lambda)}\left(e^{-(\gamma+\lambda)\tau} - e^{-\sigma\tau}\right). \tag{18}$$

Substituting into (13), we get

$$\hat{\mathcal{R}} = \left(1+\frac{r}{\sigma}\right)\left(1+\frac{r}{\gamma+\lambda}\right), \tag{19}$$

where r is the exponential growth rate. Alternatively, the reproductive number can be expressed based on the degree distribution (mean μ and variance σ^2) of a network:

$$\hat{\mathcal{R}} = \underbrace{\kappa\lambda}_{\text{average contact rate}} \times \underbrace{\frac{1}{\gamma+\lambda}}_{\text{mean effective infectious period}}, \tag{20}$$

where $\kappa = \sigma^2/\mu + \mu - 1$, referred to as the mean degree excess (Newman, 2003), describes the expected number of susceptible individuals that an average infected individual will encounter early in an outbreak. Combining the two equations, we get

$$\lambda = \frac{(\gamma+r)(\sigma+r)}{(\kappa-1)\sigma - r}, \tag{21}$$

which completes the relationship between the growth rate and the egocentric reproductive number:

$$\hat{\mathcal{R}} = \frac{\gamma+r}{\gamma\sigma/(\sigma+r) + r/\kappa}. \tag{22}$$

7.4 Population-level method for estimating generation-interval distributions from contact-tracing data

Population-level method tries to estimate the effective generation-interval distribution by reverting the inverse exponential weighting in the observed generation-interval distribution:

$$g_{\text{eff}}(\tau) \propto c_t(\tau)\exp(r\tau). \tag{23}$$

In order to do so, we first fit a gamma distribution to the observed generation-interval distributions; specifically, we estimate the mean $\bar{G}$ and shape α of a gamma distribution by maximum likelihood. Then, the effective generation-interval distribution also follows a gamma distribution with mean $\alpha/(\alpha/\bar{G} - r)$ and shape α.

7.5 Individual-level method for estimating generation-interval distributions from contact-tracing data

We model each infection i from an infected individual j as a non-homogeneous Poisson process between the time at which infector j was infected (t_j) and the censorship time (t_{censor}), where the time-varying Poisson rate at time t is equal to $\mathcal{R} g_{\text{eff}}(t - t_j)$, where $g_{\text{eff}}(t)$ is the effective generation-interval distribution (Daley and Vere-Jones, 2007). We use a gamma distribution (parameterized by its mean and shape) to model the effective generation-interval distribution. Then, the probability that an individual j infects n_j individuals between t_j and t_{censor} is equal to

$$\frac{\mathcal{R}^{n_j} \exp\big(-\mathcal{R}\, G_{\text{eff}}(t_{\text{censor}} - t_j; \theta)\big) \prod_{i=1}^{n_j} g_{\text{eff}}(s_{i,j}; \theta)}{n_j!}, \tag{24}$$

where $s_{i,j}$ is the observed generation interval between infector j and infectee i, and θ is a (vector) parameter of the generation-interval distribution g (and the corresponding cumulative distribution function G_{eff}).

The entire data likelihood of the non-homogeneous poisson process can be written as:

$$\begin{aligned} &\mathcal{L}(\mathcal{R}, \theta \,|\, \mathbf{s}, \mathbf{t}, \mathbf{n}, t_{\text{censor}}) \\ &\quad = \prod_{j=1}^{N} \left(\mathcal{R}^{n_j} \exp\big(-\mathcal{R}\, G_{\text{eff}}(t_{\text{censor}} - t_j; \theta)\big) \prod_{i=1}^{n_j} g_{\text{eff}}(s_{i,j}; \theta) \right), \end{aligned} \tag{25}$$

where N is the total number of infected individuals. Here, we estimate parameters $\mathcal{R}$ and θ by maximum likelihood. Since the estimate of $\mathcal{R}$ is sensitive to under-reporting, we use the estimated generation-interval distribution to infer the effective reproductive number from the estimated growth rate (using the Euler-Lotka equation). White and Pagano (2008) proposed a related approach based on discretized incidence reports.

7.6 Measuring the exponential growth rate

We estimate the exponential growth rate r of an epidemic from daily incidence by modeling the cumulative incidence $c(t)$ with a logistic function (Ma et al., 2014):

$$c(t) = \frac{K}{1 + [(K/c_0) - 1]\, e^{-rt}}, \tag{26}$$

where K is the final size of an epidemic and c_0 is the initial number of cases. Fitting this curve directly to cumulative incidence can lead to overly confident result (King et al., 2015); instead we fit interval incidence $x(t) = c(t+\Delta t) - c(t)$, where Δt is 1 day, to daily incidence, assuming

that daily incidence follows a negative binomial distribution. This assumption requires us to estimate the dispersion parameter θ of a negative binomial distribution. Parameters r, K, c_0, and θ are estimated by maximum likelihood. Fitting time window is defined from the last trough before the peak of an epidemic to the first day after the peak of an epidemic.

7.7 Empirical network

To simulate epidemics on a realistic network, we use the 'condensed matter physics' network from the Stanford Large Network Dataset Collection (Leskovec and Krevl, 2014). This graph describes co-authorship among anyone who submitted a paper to Condensed Matter category in the arXiv between January 1993 and April 2003 (Leskovec et al., 2007). It consists of 23133 nodes and 93497 edges. The same network was used by Trapman et al. (2016) to study how network structure affects the estimate of the reproductive number.

Authors' contributions

SWP led the literature review, wrote the first draft of the MS, performed analytic calculations and simulations; JD conceived the study and performed analytic calculations; all authors contributed to refining study design, literature review, and final MS writing. All authors gave final approval for publication.

Competing interests

The authors declare that they have no competing interests.

Funding

This work was supported by the Canadian Institutes of Health Research [funding reference number 143486].

A Appendix

A.1 Comparison of estimates of reproductive number – smaller $\mathcal{R}$

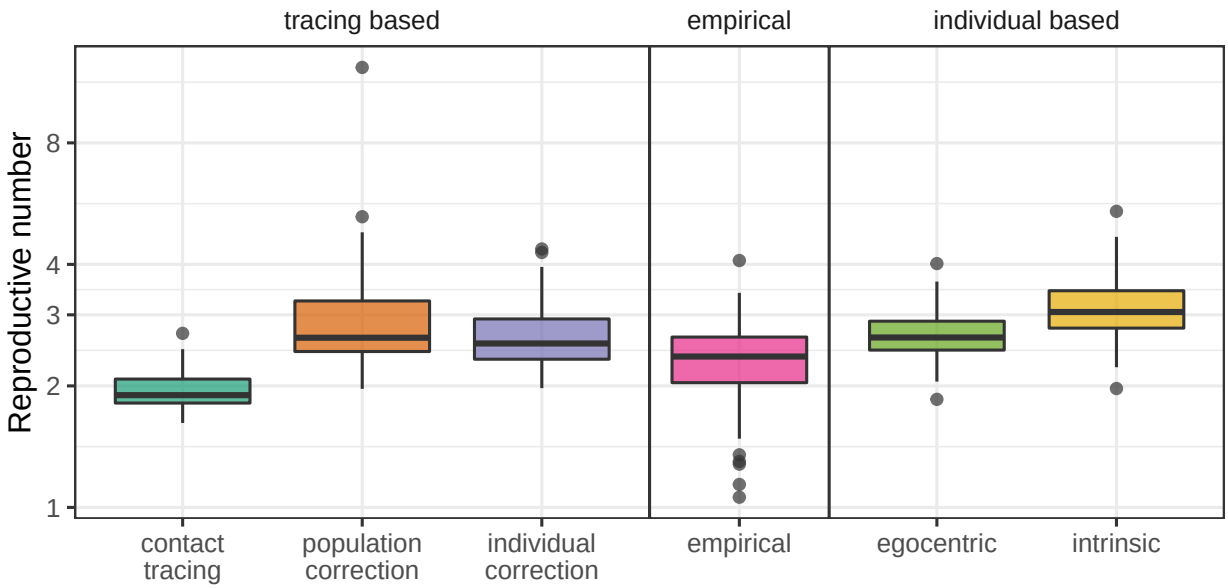

Figure A.1: **Comparison of estimates of reproductive number based on various methods.** This figure matches Fig. 4 in the main text. A smaller per-pair contact rate ($\lambda = 0.0026$ days^{-1}) is used to simulate epidemics. All other parameters are the same as in Fig. 4.

A.2 Comparison of estimates of reproductive number – Erlang distributed latent periods

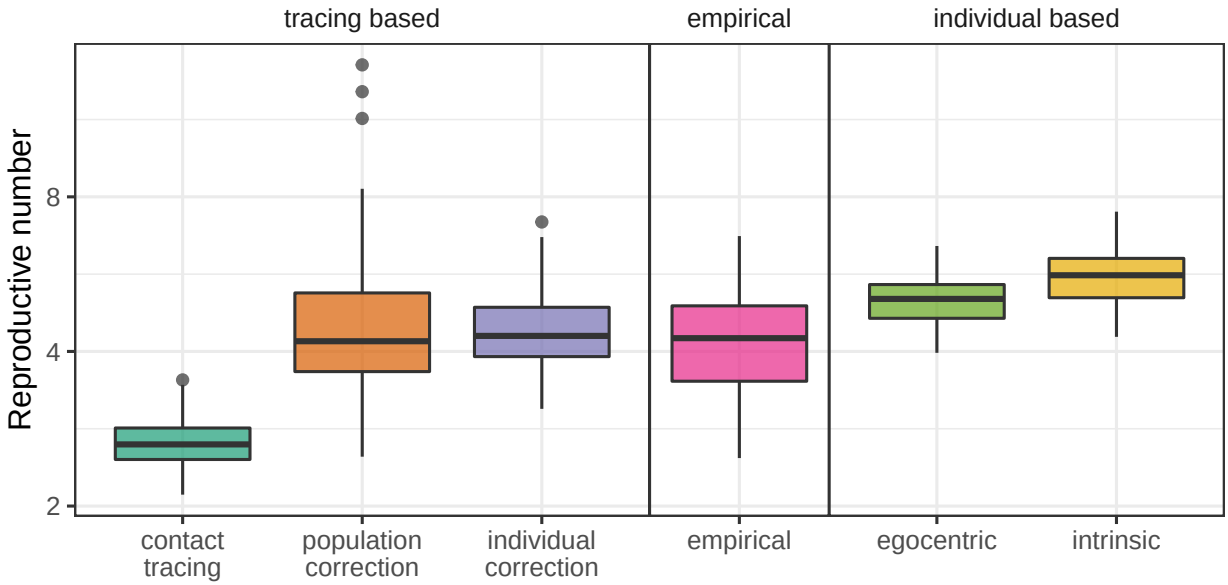

Figure A.2: **Comparison of estimates of reproductive number based on various methods.** This figure matches Fig. 4 in the main text which used a SEIR model. Here, an Erland-distributed latent period ($n_E = 2$) is used to simulate epidemics; this assumption better matches the incubation period distribution of the Ebola virus disease than the exponential assumption (WHO Ebola Response Team, 2014). All other parameters are the same as in Fig. 4.

A.3 Testing the individual-based method on simulations on a homogeneous network

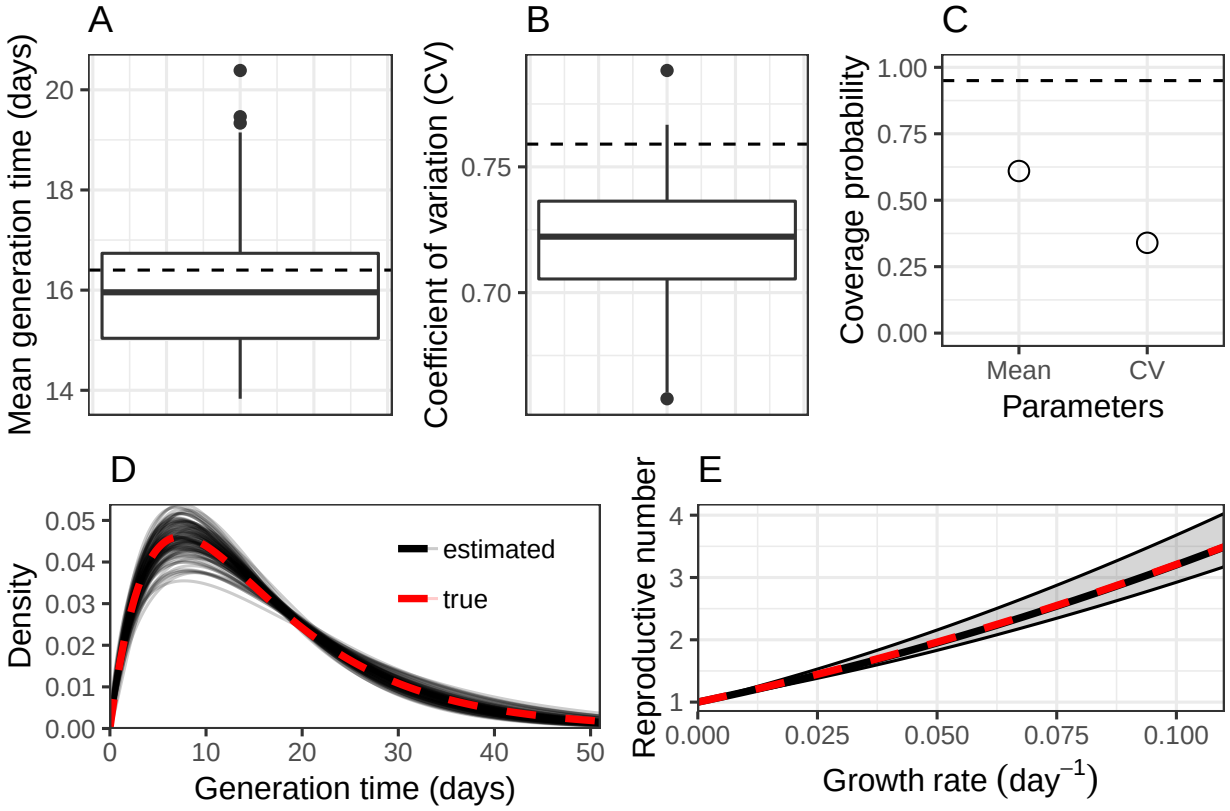

Figure A.3: **Wrong distributional assumption may result in biased estimates of the parameters of a generation-interval distribution.** We simulate a stochastic SEIR model on a homogenous network with 10^5 individuals using Ebola-like parameters (WHO Ebola Response Team, 2014): mean latent period $1/\sigma = 5$ days, mean infectious period $1/\gamma = 11.4$ days, and the basic reproductive number $\mathcal{R}_0 = 2$. Then, we apply the individual-based method based on the first 1000 infections. (A-B) A boxplot of 100 estimates of the mean generation intervals and their coefficient of variations (CV). Dashed horizontal lines represent the true value. (C) Coverage probability of the mean generation intervals and their CVs based on the 95% confidence interval. Dashed horizontal lines represent the 95% coverage probability. (D) Estimated generation-interval distributions based on the gamma approximation and a true generation-interval distribution of an SEIR model. (E) Estimated r–$\mathcal{R}$ relationships based on the gamma approximation and a true r-$\mathcal{R}$ relationship of an SEIR model. Even though there are biases in the estimates of the parameters of the generation-interval distribution, we can still get an unbiased estimate of the r–$\mathcal{R}$ relationship: a shorter mean generation interval decreases $\mathcal{R}$ whereas a tighter generation-interval distribution increases $\mathcal{R}$ (Wallinga and Lipsitch, 2007; Park et al., 2019).

References

Aldis, G. and M. Roberts (2005). An integral equation model for the control of a smallpox outbreak. *Mathematical biosciences 195*(1), 1–22.

Anderson, D. and R. Watson (1980). On the spread of a disease with gamma distributed latent and infectious periods. *Biometrika 67*(1), 191–198.

Anderson, R. M. and R. M. May (1991). *Infectious diseases of humans: dynamics and control*. Oxford university press.

Bailey, N. T. (1964). Some stochastic models for small epidemics in large populations. *Applied Statistics*, 9–19.

Ball, F., D. Mollison, and G. Scalia-Tomba (1997). Epidemics with two levels of mixing. *The Annals of Applied Probability*, 46–89.

Ball, F. and P. Neal (2002). A general model for stochastic SIR epidemics with two levels of mixing. *Mathematical biosciences 180*(1-2), 73–102.

Britton, T. and G. Scalia Tomba (2019). Estimation in emerging epidemics: Biases and remedies. *Journal of the Royal Society Interface 16*(150), 20180670.

Cauchemez, S., P.-Y. Boëlle, G. Thomas, and A.-J. Valleron (2006). Estimating in real time the efficacy of measures to control emerging communicable diseases. *American journal of epidemiology 164*(6), 591–597.

Champredon, D. and J. Dushoff (2015). Intrinsic and realized generation intervals in infectious-disease transmission. *282*(1821).

Champredon, D., J. Dushoff, and D. J. D. Earn (2018). Equivalence of the Erlang-distributed SEIR epidemic model and the renewal equation. *SIAM Journal on Applied Mathematics 78*, 3258–3278.

Chowell, G., P. W. Fenimore, M. A. Castillo-Garsow, and C. Castillo-Chavez (2003). SARS outbreaks in Ontario, Hong Kong and Singapore: the role of diagnosis and isolation as a control mechanism. *Journal of theoretical biology 224*(1), 1–8.

Chowell, G. and C. Viboud (2016). Is it growing exponentially fast?–impact of assuming exponential growth for characterizing and forecasting epidemics with initial near-exponential growth dynamics. *Infectious disease modelling 1*(1), 71–78.

Chowell, G., C. Viboud, J. M. Hyman, and L. Simonsen (2015). The Western Africa Ebola virus disease epidemic exhibits both global exponential and local polynomial growth rates. *PLoS currents 7*.

Chowell, G., C. Viboud, L. Simonsen, and S. M. Moghadas (2016). Characterizing the reproduction number of epidemics with early subexponential growth dynamics. *Journal of The Royal Society Interface 13*(123), 20160659.

Clarke, J. (1998). Contact tracing for chlamydia: data on effectiveness. *International journal of STD & AIDS 9*(4), 187–191.

Daley, D. J. and D. Vere-Jones (2007). *An introduction to the theory of point processes: volume II: general theory and structure*. Springer Science & Business Media.

Diekmann, O. and J. A. P. Heesterbeek (2000). *Mathematical epidemiology of infectious diseases: model building, analysis and interpretation*, Volume 5. John Wiley & Sons.

Diekmann, O., J. A. P. Heesterbeek, and J. A. Metz (1990). On the definition and the computation of the basic reproduction ratio R0 in models for infectious diseases in heterogeneous populations. *Journal of mathematical biology 28*(4), 365–382.

Dietz, K. (1993). The estimation of the basic reproduction number for infectious diseases. *Statistical methods in medical research 2*(1), 23–41.

Donnelly, C. A., A. C. Ghani, G. M. Leung, A. J. Hedley, C. Fraser, S. Riley, L. J. Abu-Raddad, L.-M. Ho, T.-Q. Thach, P. Chau, K.-P. Chan, T.-H. Lam, L.-Y. Tse, T. Tsang, S.-H. Liu, J. H. B. Kong, E. M. C. Lau, N. M. Ferguson, and R. M. Anderson (2003). Epidemiological determinants of spread of causal agent of severe acute respiratory syndrome in Hong Kong. *The Lancet 361*(9371), 1761–1766.

Eames, K. T. and M. J. Keeling (2003). Contact tracing and disease control. *Proceedings of the Royal Society of London. Series B: Biological Sciences 270*(1533), 2565–2571.

Gillespie, D. T. (1977). Exact stochastic simulation of coupled chemical reactions. *The journal of physical chemistry 81*(25), 2340–2361.

Heesterbeek, J. and K. Dietz (1996). The concept of R0 in epidemic theory. *Statistica Neerlandica 50*(1), 89–110.

Hens, N., L. Calatayud, S. Kurkela, T. Tamme, and J. Wallinga (2012). Robust reconstruction and analysis of outbreak data: influenza A (H1N1) v transmission in a school-based population. *American journal of epidemiology 176*(3), 196–203.

Jewell, C. P. and G. O. Roberts (2012). Enhancing Bayesian risk prediction for epidemics using contact tracing. *Biostatistics 13*(4), 567–579.

Kenah, E., M. Lipsitch, and J. M. Robins (2008). Generation interval contraction and epidemic data analysis. *Mathematical biosciences 213*(1), 71–79.

King, A. A., M. D. de Celles, F. M. Magpantay, and P. Rohani (2015). Avoidable errors in the modelling of outbreaks of emerging pathogens, with special reference to Ebola. In *Proc. R. Soc. B*, Volume 282, pp. 20150347. The Royal Society.

Kiskowski, M. and G. Chowell (2016). Modeling household and community transmission of Ebola virus disease: epidemic growth, spatial dynamics and insights for epidemic control. *Virulence 7*(2), 163–173.

Leskovec, J., J. Kleinberg, and C. Faloutsos (2007). Graph evolution: Densification and shrinking diameters. *ACM Transactions on Knowledge Discovery from Data (TKDD) 1*(1), 2.

Leskovec, J. and A. Krevl (2014). SNAP Datasets: Stanford Large Network Dataset Collection. http://snap.stanford.edu/data.

Lotka, A. J. (1907). Relation between birth rates and death rates. *Science 26*(653), 21–22.

Ma, J., J. Dushoff, B. M. Bolker, and D. J. Earn (2014). Estimating initial epidemic growth rates. *Bulletin of mathematical biology 76*(1), 245–260.

McBryde, E., I. Bergeri, C. van Gemert, J. Rotty, E. Headley, K. Simpson, R. Lester, M. Hellard, and J. E. Fielding (2009). Early transmission characteristics of influenza A (H1N1) v in Australia: Victorian state, 16 May–3 June 2009. *Eurosurveillance 14*(42), 19363.

Mills, C. E., J. M. Robins, and M. Lipsitch (2004). Transmissibility of 1918 pandemic influenza. *Nature 432*(7019), 904.

Newman, M. E. (2003). The structure and function of complex networks. *SIAM review 45*(2), 167–256.

Nishiura, H. (2010). Time variations in the generation time of an infectious disease: implications for sampling to appropriately quantify transmission potential. *Mathematical Biosciences & Engineering 7*(4), 851–869.

Nishiura, H., C. Castillo-Chavez, M. Safan, and G. Chowell (2009). Transmission potential of the new influenza A (H1N1) virus and its age-specificity in Japan. *Eurosurveillance 14*(22), 19227.

Nishiura, H. and G. Chowell (2015). Theoretical perspectives on the infectiousness of Ebola virus disease. *Theoretical Biology and Medical Modelling 12*(1), 1.

Nishiura, H., G. Chowell, M. Safan, and C. Castillo-Chavez (2010). Pros and cons of estimating the reproduction number from early epidemic growth rate of influenza A (H1N1) 2009. *Theoretical Biology and Medical Modelling 7*(1), 1.

Park, S. W., D. Champredon, J. S. Weitz, and J. Dushoff (2019). A practical generation-interval-based approach to inferring the strength of epidemics from their speed. *Epidemics*.

Roberts, M. (2004). Modelling strategies for minimizing the impact of an imported exotic infection. *Proceedings of the Royal Society of London B: Biological Sciences 271*(1555), 2411–2415.

Roberts, M. and J. Heesterbeek (2007). Model-consistent estimation of the basic reproduction number from the incidence of an emerging infection. *Journal of mathematical biology 55*(5-6), 803.

Roberts, M. G. and H. Nishiura (2011). Early estimation of the reproduction number in the presence of imported cases: pandemic influenza H1N1-2009 in New Zealand. *PLoS One 6*(5), e17835.

Scalia Tomba, G., Å. Svensson, T. Asikainen, and J. Giesecke (2010). Some model based considerations on observing generation times for communicable diseases. *Mathematical Biosciences 223*(1), 24–31.

Soetens, L., D. Klinkenberg, C. Swaan, S. Hahné, and J. Wallinga (2018). Real-time estimation of epidemiologic parameters from contact tracing data during an emerging infectious disease outbreak. *Epidemiology 29*(2), 230–236.

Svensson, Å. (2007). A note on generation times in epidemic models. *Mathematical biosciences 208*(1), 300–311.

Svensson, Å. (2015). The influence of assumptions on generation time distributions in epidemic models. *Mathematical biosciences 270*, 81–89.

Szendroi, B. and G. Csányi (2004). Polynomial epidemics and clustering in contact networks. *Proceedings of the Royal Society of London. Series B: Biological Sciences 271*(suppl_5), S364–S366.

Trapman, P., F. Ball, J.-S. Dhersin, V. C. Tran, J. Wallinga, and T. Britton (2016). Inferring R0 in emerging epidemics–the effect of common population structure is small. *Journal of the Royal Society Interface 13*(121).

Trichereau, J., C. Verret, A. Mayet, G. Manet, C. Decam, J.-B. Meynard, X. Deparis, and R. Migliani (2012). Estimation of the reproductive number for A (H1N1) pdm09 influenza among the French armed forces, September 2009–March 2010. *Journal of Infection 64*(6), 628–630.

Viboud, C., L. Simonsen, and G. Chowell (2016). A generalized-growth model to characterize the early ascending phase of infectious disease outbreaks. *Epidemics 15*, 27–37.

Wallinga, J. and M. Lipsitch (2007). How generation intervals shape the relationship between growth rates and reproductive numbers. *Proceedings of the Royal Society of London B: Biological Sciences 274*(1609), 599–604.

Wearing, H. J., P. Rohani, and M. J. Keeling (2005). Appropriate models for the management of infectious diseases. *PLoS medicine 2*(7), e174.

White, L. F. and M. Pagano (2008). A likelihood-based method for real-time estimation of the serial interval and reproductive number of an epidemic. *Statistics in medicine 27*(16), 2999–3016.

WHO Ebola Response Team (2014). Ebola virus disease in West Africa–the first 9 months of the epidemic and forward projections. *New England Journal of Medicine 371*(16), 1481–1495.